

Visualizing the BEC-BCS crossover in the two-dimensional Fermi gas: pairing gaps and dynamical response functions from *ab initio* computations

Ettore Vitali,¹ Hao Shi,¹ Mingpu Qin,¹ and Shiwei Zhang¹

¹*Department of Physics, The College of William and Mary, Williamsburg, Virginia 23187*

Experiments with ultracold atoms provide a highly controllable laboratory setting with many unique opportunities for precision exploration of quantum many-body phenomena. The nature of such systems, with strong interaction and quantum entanglement, makes reliable theoretical calculations challenging. Especially difficult are excitation and dynamical properties, which are often the most directly relevant to experiment. We carry out exact numerical calculations, by Monte Carlo sampling of imaginary-time propagation of Slater determinants, to compute the pairing gap in the two-dimensional Fermi gas from first principles. Applying state-of-art analytic continuation techniques, we obtain the spectral function, and the density and spin structure factors providing unique tools to visualize the BEC-BCS crossover. These quantities will allow for a direct comparison with experiments.

It is truly unusual when, starting from a microscopic Hamiltonian, theory can achieve an exact description of a strongly correlated fermionic system which, at the same time, can be realized in a laboratory with great precision and control. Experiments with ultracold atoms [1, 2] have provided a possibility to realize such a scenario. The accuracy that can be reached in experiments with Fermi atomic gases and optical lattices is exceptional, thus offering a unique setting to explore highly correlated quantum fermion systems. In this paper, we demonstrate that, from the theoretical side, advances in computational methods now make it feasible to obtain numerically exact results for not only equilibrium properties, but also excited states. We compute the pairing gap, spectral functions and dynamical response functions in the two-dimensional Fermi gas across the range of interactions, which will allow direct comparisons with spectroscopy or scattering experiments. The dynamical properties provide a powerful tool to probe the behavior of the system and to visualize the crossover from a gas of molecules to a BCS superfluid.

We study the Fermi gas with a zero-range attractive interaction, which has generated a great deal of research activity [1–15]. The interest of the system is very wide, ranging from condensed matter physics [6, 16] to nuclear physics, with possible important applications also in the study of neutron stars [17, 18]. This system describes experiments with a collection of atoms, for example ⁶Li, which are cooled to degeneracy in an equal mixture of two hyperfine ground states, labeled $|\uparrow\rangle$ and $|\downarrow\rangle$. Feshbach resonances allow the tuning of the interactions by varying an external magnetic field, making the system a unique laboratory to explore many-body physics [19, 20]. Starting from a weakly interacting BCS regime, where the attraction between particles induces a pairing similar to the one observed in ordinary superconductors, a crossover is observed as the interaction strength is increased, leading to a BEC regime where the Cooper pairs are tightly bound such that the system behaves as a gas of bosonic

molecules. While both the BCS and the BEC regimes are well understood, the crossover regime provides an excellent example of a strongly interacting quantum many-body system [1, 2].

We focus in particular on the two-dimensional (2D) Fermi gas, which has recently been realized experimentally using an highly anisotropic trapping potential [4, 5]. The 2D system is important, since some of the most interesting physical phenomena, such as high temperature superconductivity [21], Dirac fermions in graphene [22] and topological superconductors [23], nuclear “pasta” phases [24] in neutron stars are two-dimensional in nature. Quantum fluctuations are known to be enhanced in 2D, making it even more important to have quantitative results beyond mean-field approaches.

Experiments are just beginning to measure properties in the 2D gas [8, 11, 13, 25, 26]. An array of calculations have been performed [16, 27–31], although much less is available in 2D compared to three-dimensional systems. The most direct connection with experiments is through response functions and accurate many-body data on dynamical response at low temperatures would provide crucial and fundamental missing link. However, these are much more challenging theoretically and computationally [32].

In this paper, we develop the capabilities to obtain unbiased results for imaginary-time correlation functions in spin-balanced Fermi gas systems, using first principles auxiliary-field quantum Monte Carlo (AFQMC) [33–36] methods. This provides a unique approach to excitations and dynamical response functions. Focusing on the BEC-BCS crossover regime, we compute the pairing gap as a function of the interaction strength, the spectral function, which can be measured experimentally in photoemission spectroscopy [25], and the density and spin structure factors, which can be measured in two-photon scattering experiments [37].

As the range of the interaction in the Fermi gas system of cold atoms is much smaller than the average inter-

particle distance, the system can be modeled using a lattice Hamiltonian [38]:

$$\hat{H} = t \sum_{\vec{k}, \sigma} \varepsilon(\vec{k}) \hat{c}_{\vec{k}, \sigma}^\dagger \hat{c}_{\vec{k}, \sigma} + U \sum_i \hat{n}_{i, \uparrow} \hat{n}_{i, \downarrow}, \quad (1)$$

where the label i runs over a square lattice with $\mathcal{N}_s = L \times L$ sites hosting a total of \mathcal{N}_p fermions, half with each spin σ ($=\uparrow$ or \downarrow). The momentum $\vec{k} = (k_x, k_y)$ is defined on the reciprocal lattice with units $2\pi/L$ and $k_x, k_y \in [-\pi, \pi)$. The dispersion is $\varepsilon(\mathbf{k}) = k_x^2 + k_y^2$ and $t = \hbar^2/(2mb^2)$, with b the lattice parameter. The attractive on-site interaction U/t is tuned [29, 38] for each lattice density $n = \mathcal{N}_p/\mathcal{N}_s$ and Fermi momentum $k_F = \sqrt{2\pi n}/b$ to produce the desired scattering length a , defined as the position of the node of the zero-energy s -wave solution of the two-body problem.

The ground state wave function $|\Psi_0\rangle$ of \hat{H} is sampled using the AFQMC method [29]. For hamiltonian (1) with $U/t < 0$, the sampling is not affected by the sign problem, so that numerical results can be obtained free of any bias for each set of parameters $\{\mathcal{N}_s, \mathcal{N}_p, U/t\}$. Accelerated sampling techniques with force bias are used, together with other technical improvements [39], which greatly improves the efficiency of our calculations. This allows us to reach large system sizes in order to reliably extrapolate to the continuum and then to the thermodynamic limit [29].

Our computation of the dynamical correlation functions here relies on a new algorithm which improved the computational scaling in the calculation of imaginary-time correlation functions [40] from $\mathcal{O}(\mathcal{N}_s^3)$ in standard algorithms [41–46] to $\mathcal{O}(\mathcal{N}_s \mathcal{N}_p^2)$. The algorithm lets fluctuations related to creation/destruction operators or density/spin operators propagate in imaginary time, coupled to the stochastic evolution of the underlying AFQMC random walk or path-integral [40]. The dynamical correlation functions are obtained as suitable combinations of matrix elements involving the Slater determinants [40]. In the Fermi gas systems, the calculation is at the dilute limit, with $\mathcal{N}_s \gg \mathcal{N}_p$, so that a drastic speedup is achieved. This allows us to study lattices of $\mathcal{N}_s \sim 2000$ sites in order to, as illustrated below, reach proper convergence of the results to the realistic limit.

The exact imaginary-time correlation functions allow one to access a number of important physical quantities. We compute the pairing gap Δ from the large imaginary-time behavior of the dynamical Green's functions:

$$\begin{aligned} G^p(\vec{k}, \tau) &= \left\langle \hat{c}_{\vec{k}} e^{-\tau(\hat{H}-E_0)} \hat{c}_{\vec{k}}^\dagger \right\rangle \\ G^h(\vec{k}, \tau) &= \left\langle \hat{c}_{\vec{k}}^\dagger e^{-\tau(\hat{H}-E_0)} \hat{c}_{\vec{k}} \right\rangle, \end{aligned} \quad (2)$$

where the superscripts p and h indicate particle and hole, and E_0 is the ground-state energy. Moreover, we estimate the spectral function

$$A(\vec{k}, \omega) = \left\langle \hat{c}_{\vec{k}} \delta(\omega - \hat{H}) \hat{c}_{\vec{k}}^\dagger \right\rangle + \left\langle \hat{c}_{\vec{k}}^\dagger \delta(\omega - \hat{H}) \hat{c}_{\vec{k}} \right\rangle \quad (3)$$

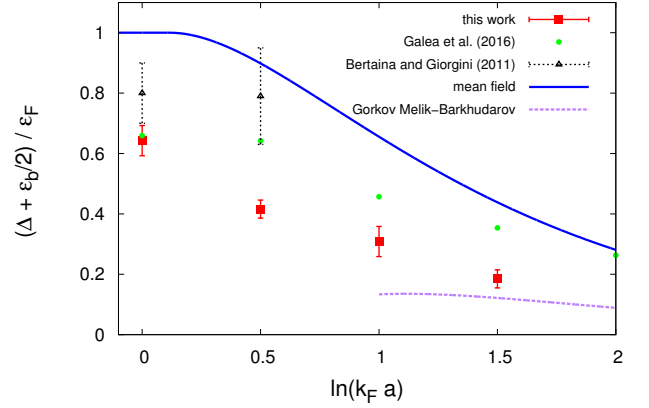


FIG. 1. (Color online) Pairing gap as a function of interaction strength, $\ln(k_F a)$. The gap values has been shifted by the binding energy, ε_b . DMC results are from Refs. [30] (circles) and [31] (triangles). BCS mean-field result is also shown for reference.

and the density and spin dynamical structure factors:

$$S^{\hat{O}}(\vec{k}, \omega) = \left\langle \hat{O}_{\vec{k}} \delta(\omega - \hat{H}) \hat{O}_{-\vec{k}} \right\rangle, \quad (4)$$

where the operator \hat{O} is $\rho_{\vec{k}} = \hat{n}_{\vec{k}, \uparrow} + \hat{n}_{\vec{k}, \downarrow}$ for density and $S_{\vec{k}} = (\hat{n}_{\vec{k}, \uparrow} - \hat{n}_{\vec{k}, \downarrow})/2$ for spin, and the brackets indicate ground-state expectations. These functions are obtained from analytic continuation of the imaginary-time Green's functions and density-density or spin-spin correlation functions, using the Genetic Inversion via Falsification of Theories (GIFT) method [47–53].

Figure 1 shows the computed pairing gap across different interaction strengths. The most standard approach to determine the pairing gap requires separate calculations corresponding to different particle numbers. While the spin-balanced calculation is free of the sign problem, the $(\mathcal{N}_p \pm 1)$ calculations are not. This makes our approach through imaginary-time Green's functions in Eq. (2) especially advantageous, since the Monte Carlo sampling remains at \mathcal{N}_p and thus sign-problem-free [40]. We are able to determine the Green's function with high statistical accuracy in the asymptotic regime in imaginary time τ , so that the behavior is dominated by an exponential whose exponent gives the quasi-particle peak at the targeted momentum \vec{k} (see Supplementary Materials). A double exponential function is used in the fit to account for any residual effects. The imaginary-time interval on which the fit is performed is stochastically varied and sampled, and multiple data sets are generated to remove statistical correlations in imaginary time within each run. The final statistical uncertainty reflects the combined effects from the AFQMC error bars and the fitting procedure. We then scan \vec{k} to locate the minimum/maximum (for the particle/hole Green's functions) for the pairing gap, as further illustrated in Fig. 2.

In Fig. 1 we also show the BCS mean-field prediction,

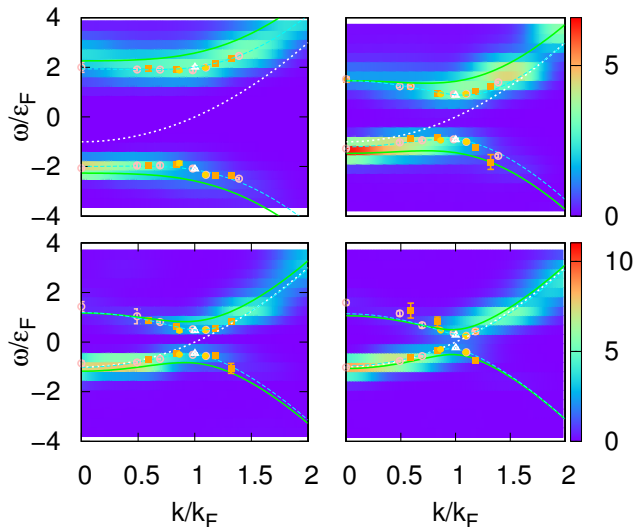


FIG. 2. (Color online) Computed quasi-particle peaks and spectral functions. The four panels are for different values of the interaction parameter: $\ln(k_F a) = 0$ (top left), $\ln(k_F a) = 0.5$ (top right), $\ln(k_F a) = 1$ (bottom left), $\ln(k_F a) = 1.5$ (bottom right). Energies are measured in units of the Fermi energy $\varepsilon_F = \hbar^2 k_F^2 / 2m$ and momenta in units of the Fermi momentum k_F . The zero of the energy is set to the chemical potential. The BCS-theory predictions for the quasi-particles energies $E_{\pm}(\vec{k})$ are shown by solid lines, while the non-interacting spectral function is given by the dotted line. The symbols are the quasi-particle peaks directly computed by AFQMC at the given momentum, for systems of 18 particles on a 25×25 lattice (orange filled squares), 26 particles on a 35×35 lattice (pink empty circles), 42 particles on a 39×39 lattice (gold filled circles) and 50 particles on a 41×41 lattice (empty triangles). Error bars are shown but some are smaller than symbol size. The light dashed lines are interpolations in the neighborhood of the minimum. The color plots give the computed spectral functions.

as well as the current best many-body results, from recent diffusion Monte Carlo (DMC) calculations [30, 31]. It is seen that our pairing gap is compatible with the DMC results on the BEC side of the crossover, but is consistently smaller for larger values of $\ln(k_F a)$. The smaller gap value is not surprising, since the DMC contains a fixed-node (FN) approximation which gives an upper bound on the computed energy. It is reasonable to expect that the trial wave function used for FN is of higher quality for the spin-balanced system compared than for the $(N_p \pm 1)$ systems, which would lead to an overestimation of the pairing gap. Our results on the BCS side are consistent with the rescaled BCS results Δ_{BCS}/e from the theory by Gorkov and Melik-Barkhudarov, which is expected to be exact in the BCS limit ($\log(k_F a) \gg 1$) [54, 55].

Figure 2 plots the computed quasi-particle peaks as a function of $k \equiv |\vec{k}|$, together with the spectral function, for four values of the interaction parameter. The zero of the energy is set equal to the chemical poten-

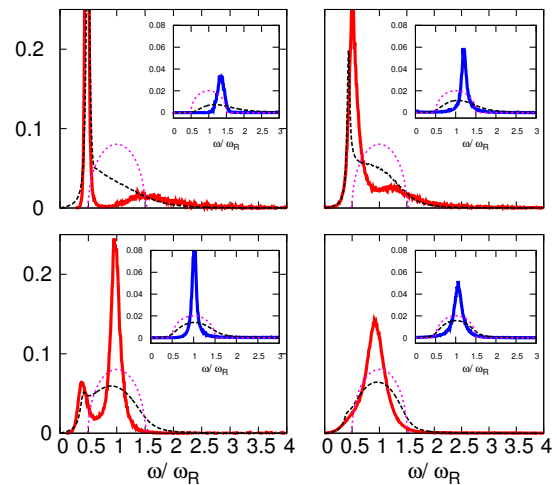


FIG. 3. (Color online) Density (main graphs) and spin (insets) dynamical structure factors at $k = 4k_F$. The four panels show four different values of the interaction parameter: $\ln(k_F a) = 0$ (top left), $\ln(k_F a) = 0.5$ (top right), $\ln(k_F a) = 1$ (bottom left), $\ln(k_F a) = 1.5$ (bottom right). Solid red lines are AFQMC results, while dashed black lines are obtained from dynamical BCS theory. The non-interacting results are also shown (dotted magenta line) in each for reference. The energies on the horizontal axes are measured in units of the atomic recoil energy, $\omega_R = \hbar^2 k^2 / 2m$.

tial, which we can compute exactly [29]. We will refer to the function $A(\vec{k}, \omega)$ as particle and hole spectral function respectively for $\omega > \mu$ and $\omega < \mu$. The particle spectral function originates from the first term on the right in Eq. (3), physically representing states available for additional particles injected into the system, while the hole spectral function, originating from the second term, contains information about states occupied by the particles in the system, which are thus accessible by the creation of holes. In each panel, we show also mean-field prediction for the quasi-particle energies [56]: $E_{\pm}(\vec{k}) = \pm \sqrt{(\hbar^2 k^2 / 2m - \mu_{BCS})^2 + \Delta_{BCS}^2}$, where Δ_{BCS} is the gap and μ_{BCS} the chemical potential in BCS theory. The non-interacting spectral function, $A^0(\vec{k}, \omega) = \delta(\omega - (\hbar^2 k^2 / 2m - \varepsilon_F))$, is also shown for reference. In the AFQMC spectral functions obtained from the GIFT analysis, shown in the color plot, quasi-particles peaks are still visible, which are broadened from many-body correlations, resulting in a non-zero imaginary part of the self-energy, and are renormalized with respect to the BCS dispersion relations. The quasi-particle peaks computed directly from AFQMC are shown by symbols. These were obtained following the procedure described in Fig. 1. Results from different system sizes are shown, which indicate convergence to the bulk limit within numerical resolution. (Separate calculations were also carried out to verify that these densities are indistinguishable from the dilute limit [29].)

The behavior of the spectral function provides a clear visualization of the BEC-BCS crossover. In the BEC regime at $\ln(k_F a) = 0$, a large gap, of the order of the energy needed to break a molecule, separates the two branches, which are roughly momentum-independent for $k \leq k_F$. A smooth evolution of the spectral function is observed. In the BCS regime at $\ln(k_F a) = 1.5$, it starts to resemble the non-interacting behavior, where a gap is still present at the Fermi momentum, as in conventional superconductors. The intermediate values of the interaction show a smooth crossover between the two regimes. Viewed in the reverse direction, gradual and significant departures from the BCS results are seen as the interaction strength is increased.

We also compute two-body dynamical correlations in imaginary time, which can again be obtained using our method with computational cost linear in \mathcal{N}_s [40]. From these, we apply analytic continuation to obtain the density and spin dynamical structure factors, $S^{\rho}(\vec{k}, \omega)$ and $S^S(\vec{k}, \omega)$, which can be measured experimentally using two-photon Bragg spectroscopy [37]. In particular, the high momentum behavior is very interesting as it provides a highly sensitive probe of the BEC-BCS crossover. We focus our attention on $k = 4k_F$, close to the value recently investigated experimentally in three-dimensions [37].

The results are plotted in Fig. 3 as functions of the frequency ω for the four values of the interaction parameter. In addition to AFQMC, we have also performed self-consistent dynamical BCS theory calculations for the same system, following the approach in Ref. [57] which studied the three-dimensional Fermi gas. The results are shown in the figure for comparison. Because the theory yields the response functions directly, it helps to provide an additional gauge on the reliability of analytic continuation analysis. We observe that the dynamical BCS theory gives results on the response functions that are qualitatively reasonable. Significant differences arise from the AFQMC results, however, for example in the peak position in the spin structure factor for strong interactions. Direct comparisons of the imaginary-time correlation functions show significant differences between AFQMC and dynamical BCS theory as well, manifesting particle correlation effects absent in the latter.

In the density response, a large peak is seen at $\omega \simeq \omega_R/2$ in the deep BEC regime. Since the particles are tightly paired to form molecules in this regime, the response of the system at high momentum is dominated by the recoil of the molecules themselves, whose mass is twice the atomic mass. In contrast, the response on the BCS side is simply a free particle recoil with the bare mass of the atoms. The behavior of the density response in the crossover regime interpolates between the two physical pictures, as is evident from Fig. 3. Starting from $\ln(k_F a) = 0$, we observe a gradual shift of the spectral weight from the dominant molecular contribution to-

wards the second peak at $\omega \simeq \omega_R$. At $\ln(k_F a) = 1$, the second peak dominates, and the molecule peak almost disappears. By $\ln(k_F a) = 1.5$, the response becomes qualitatively similar to the non-interacting one.

The spin response, on the other hand, is not sensitive to the molecular mode at $\omega \simeq \omega_R/2$, since the positive and negative fluctuations on the spin- \uparrow and spin- \downarrow particles cancel each other. However, we observe that, as it happens in three-dimensions [37], the intensity of the peak is smaller on the BEC side of the crossover, and the position of the peak is shifted towards higher energies. This corresponds to a suppression of the spin susceptibility, related to the increased energy required to remove atoms from the molecules.

In summary, we have performed *ab initio* calculations of the pairing gaps and dynamical correlation functions for the two-dimensional interacting Fermi atomic gas. Numerically exact AFQMC predictions are provided for the pairing gap. From unbiased imaginary-time correlation functions computed by AFQMC for the many-body ground state, the spectral function and the density and spin dynamical structure factors are obtained, via analytic continuation, across the BEC-BCS crossover. Much larger system sizes are reached in our simulations by the development and implementation of several technical advances. Many internal validations and self-consistency checks are performed and careful error quantifications are carried out to maximize the robustness and reliability of the results. The results will allow benchmarks of further theoretical and computational developments, and direct comparisons with experiments. The exact pairing gaps will also be crucial as an input for formulating density-functional theory in 2D [58, 59]. Excitations and dynamical correlation functions provide excellent tools for visualizing the BEC-BCS crossover. In interacting many-fermion systems in general, they connect directly with experimentally accessible measurements. Our approach opens up many new possibilities for the computational studies of strongly interacting fermionic cold atomic systems. It is hoped that the results presented here will also serve as an illustration of state-of-the-art computational capabilities, and will stimulate additional theoretical and experimental activities. The feedback from such activities will in turn spur further computations and additional developments.

We thank J. Carlson, A. Gezerlis, and Lianyi He for helpful discussions. This work was supported by NSF (Grant No. DMR-1409510). E.V. and S. Z. were also supported by the Simons Foundation. Computing was carried out at the Extreme Science and Engineering Discovery Environment (XSEDE), which is supported by National Science Foundation grant number ACI-1053575, and the computational facilities at William and Mary.

-
- [1] I. Bloch, J. Dalibard, and W. Zwerger, *Rev. Mod. Phys.* **80**, 885 (2008).
- [2] S. Giorgini, L. P. Pitaevskii, and S. Stringari, *Rev. Mod. Phys.* **80**, 1215 (2008).
- [3] J. Carlson, S.-Y. Chang, V. R. Pandharipande, and K. E. Schmidt, *Phys. Rev. Lett.* **91**, 050401 (2003).
- [4] K. Martiyanov, V. Makhalov, and A. Turlapov, *Phys. Rev. Lett.* **105**, 030404 (2010).
- [5] B. Fröhlich, M. Feld, E. Vogt, M. Koschorreck, W. Zwerger, and M. Köhl, *Phys. Rev. Lett.* **106**, 105301 (2011).
- [6] P. Magierski, G. Wlazłowski, and A. Bulgac, *Phys. Rev. Lett.* **107**, 145304 (2011).
- [7] G. Wlazłowski, P. Magierski, and J. E. Drut, *Phys. Rev. Lett.* **109**, 020406 (2012).
- [8] V. Makhalov, K. Martiyanov, and A. Turlapov, *Phys. Rev. Lett.* **112**, 045301 (2014).
- [9] W. Ong, C. Cheng, I. Arakelyan, and J. E. Thomas, *Phys. Rev. Lett.* **114**, 110403 (2015).
- [10] P. A. Murthy, I. Boettcher, L. Bayha, M. Holzmann, D. Kedar, M. Neidig, M. G. Ries, A. N. Wenz, G. Zürn, and S. Jochim, *Phys. Rev. Lett.* **115**, 010401 (2015).
- [11] M. G. Ries, A. N. Wenz, G. Zürn, L. Bayha, I. Boettcher, D. Kedar, P. A. Murthy, M. Neidig, T. Lompe, and S. Jochim, *Phys. Rev. Lett.* **114**, 230401 (2015).
- [12] K. Fenech, P. Dyke, T. Peppler, M. G. Lingham, S. Hoinka, H. Hu, and C. J. Vale, *Phys. Rev. Lett.* **116**, 045302 (2016).
- [13] I. Boettcher, L. Bayha, D. Kedar, P. A. Murthy, M. Neidig, M. G. Ries, A. N. Wenz, G. Zürn, S. Jochim, and T. Enss, *Phys. Rev. Lett.* **116**, 045303 (2016).
- [14] J. Carlson and S. Reddy, *Phys. Rev. Lett.* **95**, 060401 (2005).
- [15] Z. Luo, C. E. Berger, and J. E. Drut, *Phys. Rev. A* **93**, 033604 (2016).
- [16] M. Bauer, M. M. Parish, and T. Enss, *Phys. Rev. Lett.* **112**, 135302 (2014).
- [17] A. Gezerlis and J. Carlson, *Phys. Rev. C* **77**, 032801 (2008).
- [18] D. Lacroix, *Phys. Rev. A* **94**, 043614 (2016).
- [19] C. Chin, R. Grimm, P. Julienne, and E. Tiesinga, *Rev. Mod. Phys.* **82**, 1225 (2010).
- [20] I. Bloch, J. Dalibard, and S. Nascimbene, *Nature Physics* **8**, 267 (2012).
- [21] P. A. Lee, N. Nagaosa, and X.-G. Wen, *Rev. Mod. Phys.* **78**, 17 (2006).
- [22] A. H. Castro Neto, F. Guinea, N. M. R. Peres, K. S. Novoselov, and A. K. Geim, *Rev. Mod. Phys.* **81**, 109 (2009).
- [23] X.-L. Qi and S.-C. Zhang, *Rev. Mod. Phys.* **83**, 1057 (2011).
- [24] Y. Yu and A. Bulgac, *Phys. Rev. Lett.* **90**, 161101 (2003).
- [25] M. Feld, B. Fröhlich, E. Vogt, M. Koschorreck, and M. Köhl, *Nature* **480** (2011), 10.1038/nature10627.
- [26] C. Cheng, J. Kangara, I. Arakelyan, and J. E. Thomas, *Phys. Rev. A* **94**, 031606 (2016).
- [27] L. He, H. Lü, G. Cao, H. Hu, and X.-J. Liu, *Phys. Rev. A* **92**, 023620 (2015).
- [28] M. Klawunn, *Physics Letters A* **380**, 2650 (2016).
- [29] H. Shi, S. Chiesa, and S. Zhang, *Phys. Rev. A* **92**, 033603 (2015).
- [30] A. Galea, H. Dawkins, S. Gandolfi, and A. Gezerlis, *Phys. Rev. A* **93**, 023602 (2016).
- [31] G. Bertaina and S. Giorgini, *Phys. Rev. Lett.* **106**, 110403 (2011).
- [32] L. He, *Annals of Physics (N.Y.)* **373**, 470 (2016).
- [33] S. Zhang, *Auxiliary-Field Quantum Monte Carlo for Correlated Electron Systems*, Vol. 3 of *Emergent Phenomena in Correlated Matter: Modeling and Simulation*, Ed. E. Pavarini, E. Koch, and U. Schollwöck (Verlag des Forschungszentrum Jülich, 2013).
- [34] J. P. F. LeBlanc, A. E. Antipov, F. Becca, I. W. Bulik, G. K.-L. Chan, C.-M. Chung, Y. Deng, M. Ferrero, T. M. Henderson, C. A. Jiménez-Hoyos, E. Kozik, X.-W. Liu, A. J. Millis, N. V. Prokof'ev, M. Qin, G. E. Scuseria, H. Shi, B. V. Svistunov, L. F. Tocchio, I. S. Tupitsyn, S. R. White, S. Zhang, B.-X. Zheng, Z. Zhu, and E. Gull (Simons Collaboration on the Many-Electron Problem), *Physical Review X* **5**, 041041 (2015).
- [35] M. Qin, H. Shi, and S. Zhang, *Phys. Rev. B* **94**, 085103 (2016).
- [36] H. Shi and S. Zhang, *Phys. Rev. B* **88**, 125132 (2013).
- [37] S. Hoinka, M. Lingham, M. Delehay, and C. J. Vale, *Phys. Rev. Lett.* **109**, 050403 (2012).
- [38] F. Werner and Y. Castin, *Phys. Rev. A* **86**, 013626 (2012).
- [39] H. Shi and S. Zhang, *Phys. Rev. E* **93**, 033303 (2016).
- [40] E. Vitali, H. Shi, M. Qin, and S. Zhang, *Phys. Rev. B* **94**, 085140 (2016).
- [41] J. E. Hirsch, *Phys. Rev. B* **31**, 4403 (1985).
- [42] M. Feldbacher and F. F. Assaad, *Phys. Rev. B* **63**, 073105 (2001).
- [43] F. F. Assaad and M. Imada, *Phys. Rev. Lett.* **76**, 3176 (1996).
- [44] M. Motta, D. E. Galli, S. Moroni, and E. Vitali, *The Journal of Chemical Physics* **140**, 024107 (2014).
- [45] M. Motta, D. E. Galli, S. Moroni, and E. Vitali, *The Journal of Chemical Physics* **143**, 164108 (2015), <http://dx.doi.org/10.1063/1.4934666>.
- [46] Alhassid, Y., Bonett-Matiz, M., Liu, S., Mukherjee, A., and Nakada, H., *EPJ Web of Conferences* **69**, 00010 (2014).
- [47] E. Vitali, M. Rossi, L. Reatto, and D. E. Galli, *Phys. Rev. B* **82**, 174510 (2010).
- [48] G. Bertaina, D. E. Galli, and E. Vitali, *Advances in Physics: X* **2**, 302 (2017), <http://dx.doi.org/10.1080/23746149.2017.1288585>.
- [49] G. Bertaina, M. Motta, M. Rossi, E. Vitali, and D. E. Galli, *Phys. Rev. Lett.* **116**, 135302 (2016).
- [50] M. Motta, E. Vitali, M. Rossi, D. E. Galli, and G. Bertaina, *Phys. Rev. A* **94**, 043627 (2016).
- [51] F. Arrigoni, E. Vitali, D. E. Galli, and L. Reatto, *Low Temp. Phys.* **39**, 793 (2013).
- [52] M. Nava, D. E. Galli, S. Moroni, and E. Vitali, *Phys. Rev. B* **87**, 144506 (2013).
- [53] S. Saccani, S. Moroni, and M. Boninsegni, *Phys. Rev. Lett.* **108**, 175301 (2012).
- [54] D. S. Petrov, M. A. Baranov, and G. V. Shlyapnikov, *Phys. Rev. A* **67**, 031601 (2003).
- [55] L. P. Gorkov and M.-B. T. K., *JETP* **13**, 1018 (1961).
- [56] M. Randeria, J.-M. Duan, and L.-Y. Shieh, *Phys. Rev. Lett.* **62**, 981 (1989).
- [57] R. Combescot, M. Y. Kagan, and S. Stringari, *Phys. Rev. A* **74**, 042717 (2006).
- [58] A. Bulgac, *Annual Review of Nuclear and Particle Science* **63**, 97 (2013).

- [59] P. Zou, F. Dalfovo, R. Sharma, X.-J. Liu, and H. Hu, New Journal of Physics **18**, 113044 (2016).

Supplemental Material

Visualizing the BEC-BCS crossover in the two-dimensional Fermi gas: pairing gaps and dynamical response functions from *ab initio* computations

Ettore Vitali,¹ Hao Shi,¹ Mingpu Qin,¹ and Shiwei Zhang¹

¹*Department of Physics, The College of William and Mary, Williamsburg, Virginia 23187*

CALCULATION OF THE PAIRING GAP

We show here how we compute the pairing gap Δ starting from the dynamical Green functions in imaginary time:

$$\begin{aligned} G^p(\vec{k}, \tau) &= \langle \hat{c}_{\vec{k}} e^{-\tau(\hat{H}-E_0)} \hat{c}_{\vec{k}}^\dagger \rangle \\ G^h(\vec{k}, \tau) &= \langle \hat{c}_{\vec{k}}^\dagger e^{-\tau(\hat{H}-E_0)} \hat{c}_{\vec{k}} \rangle, \end{aligned} \quad (1)$$

The usual definition, involving the ground state energies for systems with $N_p \pm 1$ particles:

$$\begin{aligned} E_0^{N_p+1} - E_0^{N_p} &= \mu + \Delta \\ E_0^{N_p-1} - E_0^{N_p} &= -\mu + \Delta \end{aligned} \quad (2)$$

can be recast in terms of the large imaginary time behavior of the dynamical Green functions:

$$G^p(\vec{k}, \tau) \simeq c^p(\vec{k}) e^{-\tau \omega^p(\vec{k})}, \quad G^h(\vec{k}, \tau) \simeq c^h(\vec{k}) e^{-\tau \omega^h(\vec{k})} \quad (3)$$

since, for example:

$$E_0^{N_p+1} - E_0^{N_p} = \min_{\vec{k}} \omega^p(\vec{k}) \quad (4)$$

Equation (3), for a finite system, follows from the exact identity:

$$G^p(\vec{k}, \tau) = \sum_n |\langle \Psi_0^{N_p} | \hat{c}_{\vec{k}} \Psi_n^{N_p+1} \rangle|^2 e^{-\tau(E_n^{N_p+1} - E_0^{N_p})}, \quad (5)$$

with a similar one for the holes.

The key quantities to be computed are thus:

$$\omega^{p,h}(\vec{k}) - \mu = \lim_{\tau \rightarrow +\infty} \phi^{p,h}(\vec{k}, \tau) \quad (6)$$

where we introduce the notation:

$$\phi^{p,h}(\vec{k}, \tau) = -\frac{\log(G^{p,h}(\vec{k}, \tau))}{\tau} - \mu \quad (7)$$

Since we can compute the chemical potential exactly, we do not need both particle and hole correlations functions. We checked, however, that the two always give

compatible results for the pairing gap. From now on we will focus on the particles, for brevity.

$$\Delta = \min_{\vec{k}} (\omega^p(\vec{k}) - \mu) \quad (8)$$

The procedure to obtain the value of the quasi-particle dispersion $\omega^p(\vec{k})$ from $G^p(\vec{k}, \tau)$ is illustrated in the figures below. Fig. 1 shows results for a small system, where exact diagonalization is available for comparison; Fig. 2 shows results for a large system.

The main plots show, in logarithm scale, the function $G^p(\vec{k}, \tau) e^{-\tau \mu}$ for a given momentum, close to k_F . As mentioned in the main text, we average over independent simulations, in order to reduce the correlations among data for different imaginary times. We fit $G^p(\vec{k}, \tau)$ with a linear combinations of two exponentials on an interval $[\tau_0, \tau_{max}]$, the lower energy exponent yielding $\omega^p(\vec{k})$, while the higher energy exponential is meant to capture residual effects beyond (3). The uncertainty on $\omega^p(\vec{k})$ comes from a conservative combination of: (a) the AFQMC statistical error bars on $G^p(\vec{k}, \tau)$, (b) uncertainty on the fitting parameters and (c) dependence on the choice of the interval $[\tau_0, \tau_{max}]$, τ_0 being randomly sampled in the large imaginary time tail of $G^p(\vec{k}, \tau)$.

In the insets of the two plots we show the function $\phi^p(\vec{k}, \tau)$ in the large imaginary time limit, together with the computed $\omega^p(\vec{k})$. We plot several examples of fitted functions, whose limits for $\tau \rightarrow \infty$ are used to compute $\omega^p(\vec{k})$ and the error bar. For the small system, we also show the exact diagonalization result, which is in excellent agreement with the AFQMC result.

The consistency seen between the the small system in Fig. 1 and the large system in Fig. 2 is a further indication of the robustness of our calculations.

Finally, in table I we list the values of the computed $\omega^{p,h}(\vec{k})$ in a neighborhood of the minimum, which will provide valuable benchmark.

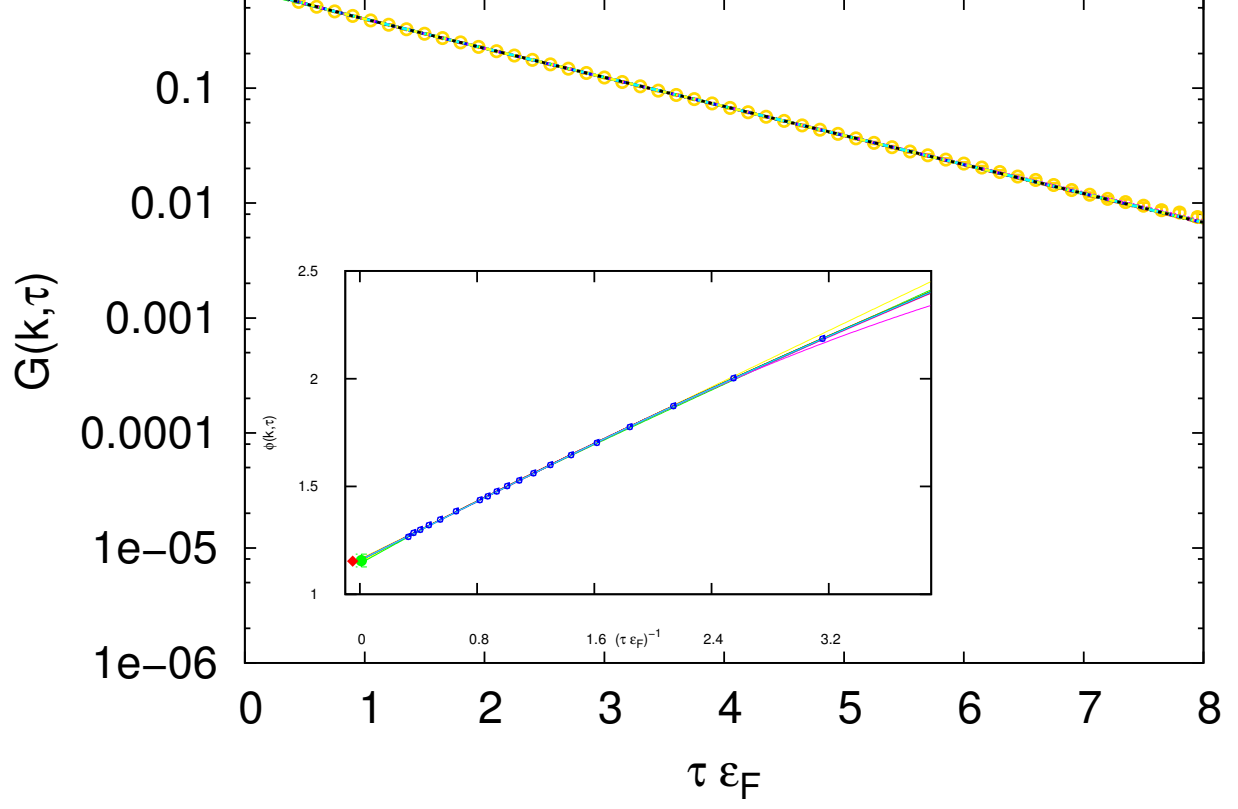


FIG. 1. (color online) $G^p(\vec{k}, \tau)e^{-\tau\mu}$ from AFQMC for a system of $\mathcal{N}_p = 4$ particles on a $L \times L = 5 \times 5$ lattice, $\vec{k} = \frac{2\pi}{L}(1, 0)$. Also shown are several double exponential fits. The inset shows $\phi^p(\vec{k}, \tau)$ in the large τ limit. The double exponential fits are also shown. The circle represents the AFQMC result with error-bar ($\Delta/\varepsilon_F = 1.156 \pm 0.03$), while the diamond represents the exact diagonalization result ($\Delta/\varepsilon_F = 1.153$). Error bars on $\phi^p(\vec{k}, \tau)$ are smaller than the symbols size.

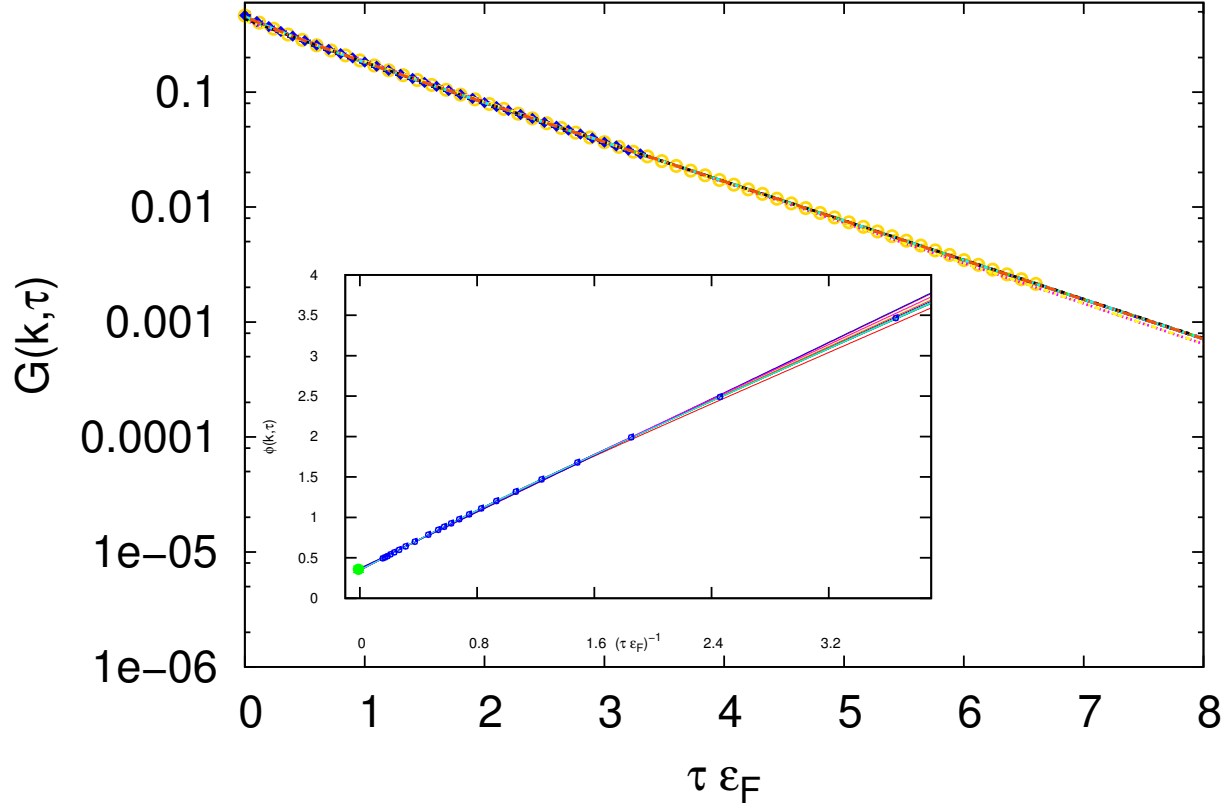


FIG. 2. (color online) $G^p(\vec{k}, \tau)e^{-\tau\mu}$ for a system of $\mathcal{N}_p = 26$ particles on a $L \times L = 35 \times 35$ lattice, $|\vec{k}|/k_F = 0.98$. The function $G^p(\vec{k}, \tau)e^{-\tau\mu}$ has been computed as an average over multiple independent AFQMC runs to avoid biases due to autocorrelations in imaginary time. Also shown are several double exponential fits. The inset shows $\phi^p(\vec{k}, \tau)$ in the large τ limit. The double exponential fits are shown, also here. The circle represents the AFQMC result with error-bar. Error bars on $\phi^p(\vec{k}, \tau)$ are smaller than the symbols size.

TABLE I. Quasi-particles and quasi-holes dispersions

$\log(k_F a)$	$\varepsilon_B/2\varepsilon_F$	$ \vec{k} /k_F$	$(\omega^p(\vec{k}) - \mu)/\varepsilon_F$	$(\omega^h(\vec{k}) + \mu)/\varepsilon_F$
0	-1.26	0.00	2.0(2)	2.06(6)
0	-1.26	0.49	1.91(5)	1.95(7)
0	-1.26	0.59	1.94(5)	1.96(5)
0	-1.26	0.70	1.91(3)	1.95(7)
0	-1.26	0.84	1.92(7)	1.90(7)
0	-1.26	0.86	1.88(6)	1.86(8)
0	-1.26	0.98	1.88(8)	2.08(8)
0	-1.26	1.00	1.99(3)	2.12(5)
0	-1.26	1.09	1.99(4)	2.33(4)
0	-1.26	1.10	1.99(4)	2.33(4)
0.5	-0.46	0.84	0.93(6)	0.84(7)
0.5	-0.46	0.86	0.94(4)	0.92(4)
0.5	-0.46	0.98	0.92(5)	0.94(5)
0.5	-0.46	1.00	0.97(1)	0.87(1)
0.5	-0.46	1.09	1.00(5)	0.93(5)
0.5	-0.46	1.10	0.93(5)	1.00(5)
0.5	-0.46	1.18	1.02(7)	1.21(7)
1.0	-0.17	0.84	0.64(5)	0.45(2)
1.0	-0.17	0.86	0.47(6)	0.50(1)
1.0	-0.17	0.98	0.52(3)	0.51(1)
1.0	-0.17	1.00	0.45(2)	0.45(1)
1.0	-0.17	1.09	0.49(4)	0.55(1)
1.5	-0.06	0.86	0.47(1)	0.29(2)
1.5	-0.06	0.98	0.36(4)	0.26(3)
1.5	-0.06	1.00	0.27(2)	0.23(2)
1.5	-0.06	1.09	0.26(3)	0.27(3)